

Continuous-wave and pulsed EPR study of the negatively charged silicon vacancy with $S = \frac{3}{2}$ and C_{3v} symmetry in n -type $4H$ -SiC

N. Mizuochi,^{1,*} S. Yamasaki,² H. Takizawa,³ N. Morishita,³ T. Ohshima,³ H. Itoh,³ and J. Isoya^{1,†}

¹University of Library and Information Science, 1-2 Kasuga, Tsukuba-City, Ibaraki 305-8550, Japan

²National Institute of Advanced Industrial Science and Technology (AIST), Advanced Semiconductor Research Center,

AIST Tsukuba Central 4, Tsukuba-city, Ibaraki 305-8562, Japan

³Japan Atomic Energy Research Institute, 1233 Watanuki, Takasaki-City, Gunma 370-1292, Japan

(Received 24 April 2002; revised manuscript received 19 July 2002; published 5 December 2002)

The T_{V2a} center, which was suggested to be the excited triplet state ($S=1$) of the neutral silicon vacancy related defect [Sörman *et al.*, Phys. Rev. B **61**, 2613 (2000)] in the electron-irradiated n -type $4H$ -SiC has been studied by continuous wave and pulsed electron paramagnetic resonance (EPR). The spin multiplicity of T_{V2a} has been determined to be quartet ($S=3/2$) by the nutation method of pulsed EPR technique. From the temperature dependence of the signal intensity, it has been revealed that the T_{V2a} spectrum is arising from an electronic ground state. From the measurement of the ^{13}C hyperfine interactions of the nearest neighbors which has been enabled by the selective enhancement of the T_{V2a} signals through the spin polarization by a laser light (808 nm) illumination, the center is unambiguously identified to be a single silicon vacancy. It is proposed that the center is a negatively charged silicon vacancy of C_{3v} symmetry with the crystal field distorted slightly from regular tetrahedron. The triply degenerate t_2 state of an electronic configuration $a_1^2 t_2^3$ under T_d symmetry splits into a_1 and e by the distortion to C_{3v} . The high spin configuration [$a_1 e^2$ or $e^2 a_1$] which reduces the electron repulsion energy is preferred rather than the low spin configuration expected from the symmetry-lowering crystal field alone. The important role of the many-electron effect in determining the ground-state configuration is demonstrated clearly by T_{V2a} in which the electron-electron interactions (the electronic repulsion and the electron exchange) compete against the crystal-field splitting.

DOI: 10.1103/PhysRevB.66.235202

PACS number(s): 61.72.Ji, 76.30.Mi

I. INTRODUCTION

In crystalline semiconductors, lattice vacancies are one of the most important intrinsic defects that might be introduced during crystal growth and material processing such as ion implantation. Electron paramagnetic resonance (EPR) is one of the most powerful methods to elucidate the geometric and electronic structures of vacancies. Irradiating with energetic particles produces a concentration of vacancies sufficient for a detailed structure determination. Selecting the kind and the concentration of major impurities varies the charge of vacancy.

The structure relaxation of vacancy is determined by a modification of the neighboring bonds. In a simple one-electron model of a single vacancy of tetrahedral semiconductors, defect molecular orbitals, which are linear combinations of the dangling bond orbitals of four atoms around the vacancy, split into an a_1 singlet and a t_2 triplet under T_d symmetry.¹ The electronic configuration of the ground state of negatively charged vacancy (V^-) is $a_1^2 t_2^3$. From the determination of the effective spin of $S=3/2$ and the T_d symmetry by using EPR and electron nuclear double resonance (ENDOR) techniques, the ground state of V^- in diamond ($E_g = 5.5\text{eV}$) was identified to be 4A_2 .² In V^- of diamond, the repulsion among the highly localized three t_2 electrons is lowered by occupying each of three different orbitals. The orbitally nondegenerate 4A_2 state is not subject to a Jahn-Teller distortion. In silicon ($E_g = 1.1\text{eV}$), V^- has a C_{2v} symmetry with $S=1/2$.³ The energy stabilization is achieved by the Jahn-Teller distortion, while the electronic repulsion is

lowered by an extensive delocalization. The extent of the wave function along the [110] chain was confirmed by ENDOR measurements.⁴

Silicon carbide (SiC) is a promising material for high-frequency, high-temperature, and high-power devices. The quality of SiC crystals have been significantly improved by recent developments of the crystal growth techniques. SiC has many polytypes differing in the stacking sequence of Si-C bilayers. Technologically important polytypes are $3C$ - (T_d^2 , $E_g = 2.39\text{ eV}$),⁵ $4H$ - (C_{6v}^4 , $E_g = 3.26\text{ eV}$),⁵ and $6H$ -SiC (C_{6v}^4 , $E_g = 3.02\text{ eV}$).⁵ In $3C$ -SiC, each of silicon and carbon has one site. In the hexagonal crystals (nH -), there are $n/2$ inequivalent sites for each of silicon and carbon. In $4H$ -SiC, each of silicon and carbon has two inequivalent sites with either hexagonal or quasicubic character.

The single negatively charged vacancy V_{Si}^- was identified in $3C$ -,⁶ $4H$ -,⁷ and $6H$ -SiC.⁸ The vacancies are observable after electron irradiation at room temperature, and anneal out around 800°C .⁹ From the isotropic g factor and the absence of the zero-field splitting (ZFS), the ground state is assigned to be spin quartet ($S=3/2$) state 4A_2 . In the T_d symmetry, all three $\Delta M_S = \pm 1$ transitions of $S=3/2$ are superimposed since the ZFS vanishes. In V_{Si}^- of $3C$ -SiC, the tetrahedral arrangement of the nearest neighbors (i.e., four carbon atoms around the vacancy) was confirmed from the angular dependence of the ^{13}C hyperfine lines.⁶ In V_{Si}^- of $4H$ -SiC, the spin multiplicity was determined to be quartet ($S=3/2$) by ENDOR measurements since the ENDOR frequencies $h\nu = |M_S A_{\text{eff}} g_n \beta_n B|$ do depend on M_S .⁷ Even in the hexagonal lattice such as $4H$ - and $6H$ -SiC, it has been suggested that

the spin quartet state should be originated from the predominantly tetrahedral character of the local symmetry. The high spin state with no symmetry lowering was also suggested by theoretical studies.^{10–12}

An $S=1$ ground state is expected for neutral vacancy ($V_{Si}^0, a_1^2 t_2^2$) and double negative vacancy ($V_{Si}^{-2}, a_1^2 t_2^4$) from a theoretical study.¹¹ The vacancy-related defects to which the effective spin of $S=1$ was assigned from the small ZFS exhibiting C_{3v} symmetry were observed in $4H$ - and $6H$ -SiC by EPR,^{13–15} and by optically detected magnetic resonance (ODMR).¹⁶ It was suggested that these spectra were arising from the excited triplet state of the carbon-silicon vacancy pair^{13,14} and from the excited triplet state of single vacancy-related defects.^{15,16} Those observed in $4H$ -SiC were labeled T_{V2a} , and T_{V2b} .¹⁶

In this work, T_{V2a} in the electron-irradiated n -type $4H$ -SiC has been studied by continuous wave (cw) and pulsed EPR. We will show that T_{V2a} is a negatively charged silicon vacancy with a quartet ($S=3/2$) ground state similar to V_{Si}^- of the T_d symmetry but having the C_{3v} symmetry.

Vacancies occur in various charge states. For identifying the charge state, it is crucial to determine the spin multiplicity. The effective spin of T_{V2a} and T_{V2b} was considered to be $S=1$ from the observation of the two lines split by the ZFS in EPR and ODMR. However, in EPR experiments, it might not be trivial to rule out the assignment of $S=3/2$ when the central part of the spectrum is superimposed with dominantly strong signals from other defects. In our preliminary report,¹⁷ we used the assignment of $S=1$ for T_{V2a} and T_{V2b} . In ODMR experiments, the signals of T_{V2a} and T_{V2b} could be selectively extracted by tuning to their optical transitions. However, the intensity of the $|S, M_S\rangle = |3/2, 1/2\rangle \leftrightarrow |3/2, -1/2\rangle$ transition might happen to be suppressed when the signal is detected through some polarization mechanism and when S and M_S are good quantum numbers.^{18,19} We will show that the nutation method of the pulsed EPR technique^{20,21} has made it possible to measure the effective spin of both T_{V2a} and T_{V2b} to be $S=3/2$.

Both T_{V2a} and T_{V2b} were suggested to be silicon vacancy related defects since the shoulders in the lineshape are similar to those arising from ^{29}Si ($I=1/2$, 4.7%) hyperfine interaction of the next-nearest-neighbor (NNN) silicon in V_{Si}^- .¹⁶ For identification of the single vacancy, it is crucial to observe hyperfine interactions of the nearest-neighbor (NN) atoms which are located immediately around the vacancy. To disentangle the angular dependence of the weak ^{13}C ($I=1/2$, natural abundance 1.1%) hyperfine lines in the presence of superimposing many other signals, selective enhancement of the signals concerned is desirable. We have achieved a selective enhancement of the T_{V2a} spectrum through a spin polarization of the multiplet sublevels by illuminating with a laser light and could measure the ^{13}C hyperfine interactions of the NN carbon sites.¹⁷

In V_{Si}^- of the T_d symmetry, the high spin state $S=3/2$ is arising from three electrons in the threefold degenerate t_2 state. In a C_{3v} symmetry, the t_2 triplet splits into an a_1 singlet and an e doublet. We will demonstrate that the T_{V2a} center is the case in which the high spin $S=3/2$ configuration

is arising from non-degenerate orbitals split by the symmetry-lowering crystal field.

II. EXPERIMENT

The samples used in our experiments were single crystal-line n -type $4H$ -SiC (Nippon Steel: nitrogen dopant) with the carrier concentration of circa $1 \times 10^{17}/\text{cm}^3$. The sample whose thickness is 1.5 mm was cut into a size ($3 \times 15 \text{ mm}^2$) appropriate for our EPR measurements in X band. The crystal was irradiated by 3-MeV electrons with the total fluence $4 \times 10^{18} e/\text{cm}^2$. The sample was placed on a water-cooled holder so as to avoid beam heating and was kept below 330 K during the electron irradiation.

Pulsed EPR experiments were carried out at room temperature on a Bruker ELEXSYS X -band spectrometer. The continuous wave (cw) EPR spectra were measured on a Bruker ESP 300 X -band spectrometer. The temperature was controlled by using an ESR-900 (Oxford Instruments). The calibration of the magnetic field was carried out by measuring simultaneously at room temperature the sample and the perylene cation in conc. H_2SO_4 ($g=2.002569 \pm 0.000006$) (Refs. 22 and 23) sealed in the capillary which was comounted with the sample. The EPR signal of Cr^{3+} in a single crystal of ruby²⁴ comounted with the sample was used as the reference of the spin concentration and was used to monitor the variation of the Q factor of the cavity during measuring the temperature dependence of the signal intensity. The signal intensity was estimated by double integration of the first derivative signal.

In the laser irradiation experiments, the crystal was illuminated with a continuous wave laser light (808 nm, 1.53 eV) of a Coherent fiber array packaged (FAP) system with a 10-W output during the EPR measurements. The laser light was introduced into the cavity through an optical fiber.

III. RESULTS AND DISCUSSION

A. Determination of the spin multiplicity

The EPR spectrum of the electron irradiated n - $4H$ -SiC when the magnetic field is parallel to the c axis ($\mathbf{B}_0 \parallel [0001]$) is shown in Fig. 1(a). In the central part of the spectrum, the negatively charged silicon vacancy (V_{Si}^- , $g=2.0028$) (Ref. 25) is observed. In both sides of the V_{Si}^- , there are the EPR signals labeled T_{V2a} and T_{V2b} which were observed previously by ODMR.¹⁶ The two-line feature of T_{V2a} and T_{V2b} was ascribed to the ZFS of $S=1$. As described below, the C_{3v} symmetry and the EPR parameters g and D , under an assumption that $S=1$, and the ^{29}Si hyperfine splitting arising from 12 NNN's which have been determined from the angular dependence of the line positions, agree with those reported in the literature.¹⁶

In the case of V_{Si}^- ($S=3/2$) in $3C$ -, $4H$ -, and $6H$ -SiC, the EPR spectrum consists of a single line as in the case of an EPR spectrum of $S=1/2$, since the ZFS for $S \geq 1$ vanishes under the T_d symmetry. In a lower symmetry, the effective spin S is usually determined from the observation of ZFS in which the EPR spectrum splits into $2S+1$ lines of $\Delta M_S = \pm 1$ transitions when the ZFS is much smaller in magnitude

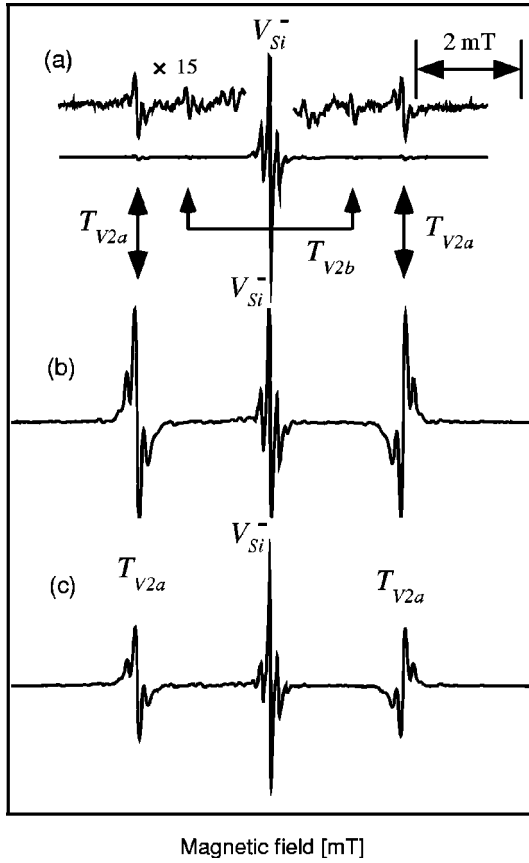


FIG. 1. The EPR spectrum of the electron-irradiated n -type 4H-SiC taken with the magnetic field along the [0001] axis (microwave power $0.2 \mu\text{W}$, amplitude of 100 kHz, field modulation 0.03 mT). (a) The spectrum in the dark at room temperature (microwave frequency $\nu = 9.4383$ GHz). The upper spectrum is the expanded spectrum. (b) The spectrum under illumination with the laser light (808 nm, 10 W) at 160 K ($\nu = 9.41628$ GHz). (c) The spectrum under illumination with the laser light (808 nm, 3 W) at 160 K.

than the microwave energy. However, when the central line arising from the $|S, M_S\rangle = |3/2, 1/2\rangle \leftrightarrow |3/2, -1/2\rangle$ transition of $S=3/2$ is hidden by an overlap of strong signals from other centers, the effective spin might be assumed to be $S=1$. The angular dependence of the line positions of the outer two lines, $|3/2, \pm 3/2\rangle \leftrightarrow |3/2, \pm 1/2\rangle$, might be well described as those of the $|1, \pm 1\rangle \leftrightarrow |1, 0\rangle$ transitions of an $S=1$ case. As shown below, we have determined that, in both T_{V2a} and T_{V2b} , the two lines are $|3/2, \pm 3/2\rangle \leftrightarrow |3/2, \pm 1/2\rangle$ transitions by applying the nutation method of pulsed technique.

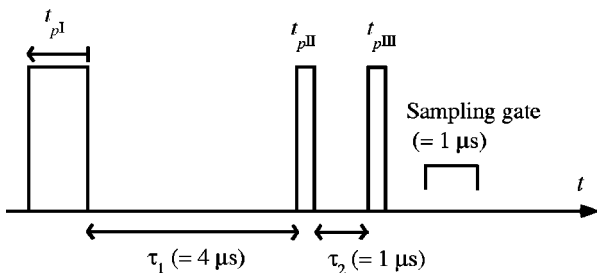


FIG. 2. The pulse sequence used in the nutation experiment.

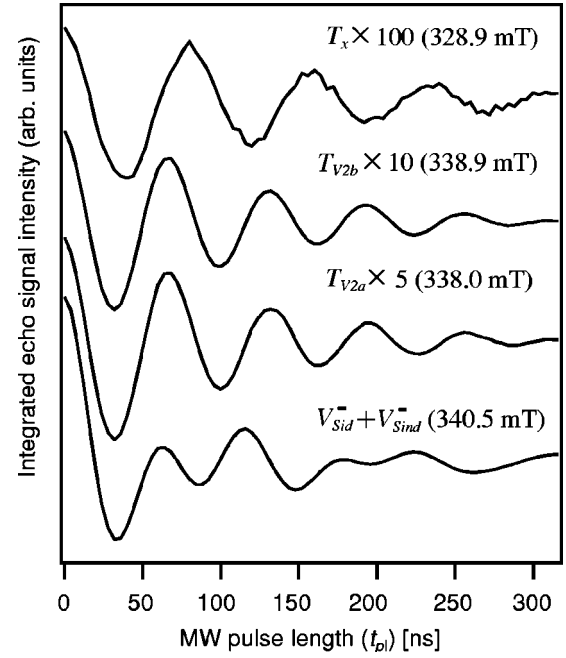


FIG. 3. Spin nutation of paramagnetic centers in electron-irradiated n -type-4H-SiC. The integrated echo intensity as a function of t_{pI} is shown. The signal intensities of T_x , T_{V2a} , and T_{V2b} are expanded by the factors indicated.

Pulsed EPR measures an EPR signal in the time domain following a pulse or a series of pulses. The behavior of the magnetization \mathbf{M} is described by using a coordinate system rotating with the microwave frequency around the external magnetic field \mathbf{B}_0 . At the resonance condition, the microwave pulse (duration t_p , amplitude B_1) rotates the magnetization in the yz plane through the angle $(g\beta_e B_1/\hbar)t_p = \omega_n t_p$ from the z axis, where ω_n is the nutation frequency. In an $S=1/2$ system, $\omega_n = \omega_1 = g\beta_e B_1/\hbar$. If all transitions of $S \geq 1$ are excited by the microwave pulse, $\omega_n = \omega_1$.^{19-21,26} If only an $|S, M_S - 1\rangle \leftrightarrow |S, M_S\rangle$ transition in the spectrum is excited, the nutation frequency ω_n of this transition is described as^{19-21,26}

$$\omega_n = \sqrt{S(S+1) - M_S(M_S - 1)} \omega_1. \quad (1)$$

If only one of the $|1, \pm 1\rangle \leftrightarrow |1, 0\rangle$ transitions of $S=1$ is excited, $\omega_n = \sqrt{2} \omega_1$. If only one of the outer two lines of $S=3/2$, $|3/2, \pm 3/2\rangle \leftrightarrow |3/2, \pm 1/2\rangle$ is excited, $\omega_n = \sqrt{3} \omega_1$, and if only the $|3/2, 1/2\rangle \leftrightarrow |3/2, -1/2\rangle$ transition is excited, $\omega_n = 2\omega_1$.

We used a three-pulse sequence ($t_{pI} - \tau_1 - t_{pII} - \tau_2 - t_{pIII} - \text{echo}$), as shown in Fig. 2. As a result of the nutation driven by the microwave pulse with the duration t_{pI} , the z component of the magnetization M_z is $M_z \propto M_0 \cos(\omega_n t_{pI})$, where M_0 is an initial magnetization. The M_z is stored during the interval τ_1 ($4 \mu\text{s}$, fixed) which is sufficiently shorter than the spin-lattice relaxation time. The second and third pulses ($t_{pII} = t_{pIII} = 20$ ns, $\tau_2 = 1 \mu\text{s}$, fixed) were used to monitor M_z in the form of an echo. In the two-dimensional (2D) nutation experiment, the time-sweep mode spectra, echo intensity vs t_{pI} was measured as a function of the ex-

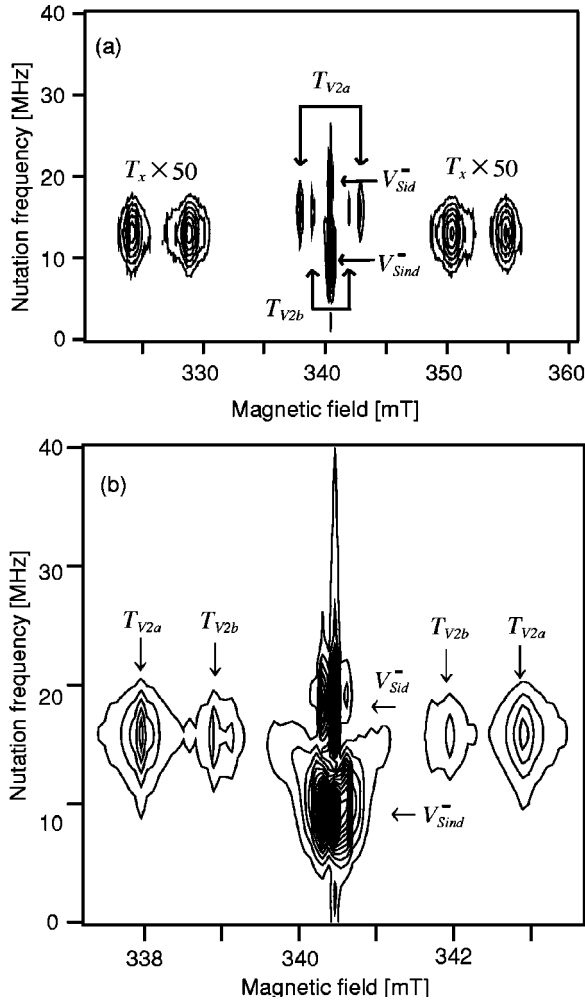


FIG. 4. The 2D nutation spectrum taken with the magnetic field along the [0001] axis at room temperature. (a) The contour plot of the nutation intensity vs. nutation frequency and the external magnetic field. The intensity of T_x is expanded. (b) The central part obtained by zooming in on (a).

ternal magnetic field strength B_0 . The pulse duration t_{p1} was varied in 80 steps with 4-ns increments. The magnetic field B_0 was incremented in 512 steps. In accumulation, two-step phase cycling $[0, 0, 0]-[0, \pi, 0]$ was employed. The echo intensity was obtained by integrating the echo shape sampled in the range of 1000 ns with 8-ns step. At the orientation of the crystal where \mathbf{B}_0 was nearly along [0001], the signals from T_{V2a} , T_{V2b} , and V_{Si}^- , and an unidentified center (denoted T_x here) were observed. The examples of the inte-

grated echo intensity with respect to t_{p1} are illustrated in Fig. 3. For each magnetic field, the integrated echo intensity of the t_{p1} scan was apodized using a sine-bell function, was expanded to 512 points by zero filling, and was Fourier-transformed to give nutation frequencies and corresponding intensities. The contour plot of the 2D nutation data, in which the nutation intensities were obtained as a function of the 2D array (ω_n, B_0) , is shown in Fig. 4. The small splitting in the magnetic field positions of T_x was caused by a misalignment. We note the nutation frequency peaks centered at 9.2, 13.0, 15.9, and 18.3 MHz, respectively. Since these frequencies correspond to the ratio $1:\sqrt{2}:\sqrt{3}:2$, the transitions are assigned as shown in Table I. Thus, for both T_{V2a} and T_{V2b} , the spin multiplicity has been determined to be quartet ($S=3/2$). The effective spin of T_x was determined to be $S=1$.

For V_{Si}^- , the nutation frequencies of ω_1 and $2\omega_1$ were observed. The frequency ω_1 corresponds to a non-distorted configuration (labeled V_{Sind}^-) in which all three $\Delta M_S = \pm 1$ transitions are excited by the microwave pulse. The frequency $2\omega_1$ corresponds to a slightly distorted configuration (labeled V_{Sid}^-) in which only the $|3/2, 1/2\rangle \leftrightarrow |3/2, -1/2\rangle$ transition is excited because the ZFS is larger than B_1 . For the slightly distorted configuration, the EPR signals corresponding to the $|3/2, \pm 3/2\rangle \leftrightarrow |3/2, \pm 1/2\rangle$ transitions were not observed in both cw and pulsed measurements. It is likely that both amplitude and direction of the ZFS are distributed, and the EPR signals are too broad to be detected as separate signals.

B. Temperature dependence of signal intensity

There have been controversies whether T_{V2a} and T_{V2b} are the ground^{11,15} or excited state.¹⁶ As shown below, we have confirmed that both spectra T_{V2a} and T_{V2b} are arising from the ground state from the temperature dependence of the EPR signal intensity. The temperature dependence of the EPR signal intensity at thermal equilibrium is caused by the population among the spin levels and by the temperature dependence of the concentration of the defects at the particular electronic state from which the EPR signal is observed.

We measured the temperature dependence of the signal intensity of V_{Si}^- , T_{V2a} , and T_{V2b} in the temperature range between 125 and 300 K. As seen from Fig. 5, the signal intensity decreases as the temperature increases in all three defects. Under 125 K, the intensity of the T_{V2a} and the T_{V2b} signals were not free from the saturation effect even at the lowest power available in our equipment. Both the T_{V2a} and

TABLE I. The nutation frequencies and their assignments.

Defect center	Observed ω_n (MHz)	Assignment of the transitions	Predicted ω_n
T_{V2a} and T_{V2b}	15.9	$ S, M_S\rangle = 3/2, \pm 3/2\rangle \leftrightarrow 3/2, \pm 1/2\rangle$	$\sqrt{3}\omega_1$
V_{Sid}^-	18.3	$ 3/2, 1/2\rangle \leftrightarrow 3/2, -1/2\rangle$	$2\omega_1$
V_{Sind}^-	9.2	$ 3/2, \pm 3/2\rangle \leftrightarrow 3/2, \pm 1/2\rangle$ and $ 3/2, 1/2\rangle \leftrightarrow 3/2, -1/2\rangle$	ω_1
T_x	13.0	$ 1, \pm 1\rangle \leftrightarrow 1, 0\rangle$	$\sqrt{2}\omega_1$

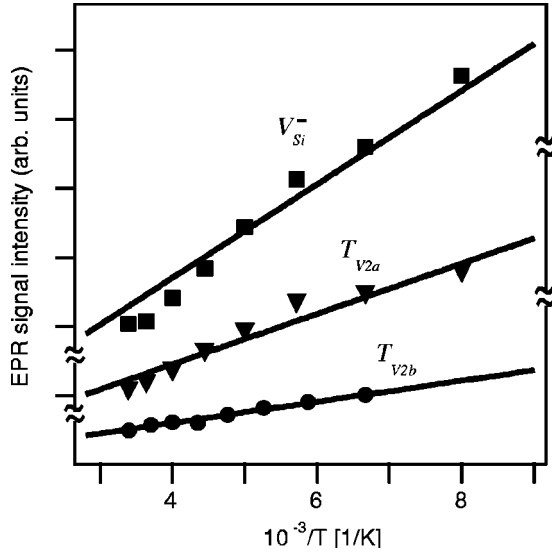


FIG. 5. The temperature dependence of the EPR signal intensities. Filled squares, triangles, and circles indicate the observed signal intensities of V_{Si}^- , T_{V2a} , and T_{V2b} , respectively. For both T_{V2a} and T_{V2b} , the intensities were obtained as the sum of the low- and high-field lines. Solid lines were obtained by the least-squares fitting using Eq. (2).

T_{V2b} signals were observed at 10 K, however, were severely distorted due to the passage effect.

In estimating the temperature dependence of an EPR signal from a quartet system, generally, it needs to be considered that the energy of the four M_S levels is not equally spaced. In T_{V2a} and T_{V2b} , the zero-field splitting is smaller by two orders of magnitude than the Zeeman energy at the microwave frequency of the X band. If we assume that the temperature dependences of the EPR signals of T_{V2a} and T_{V2b} are caused by the populations among the M_S levels of the electronic ground quartet state ($S=3/2$), the temperature dependence of the intensities of the three $\Delta M_S = \pm 1$ transitions (the intensity I_j at the resonance field B_j , $j=1, 2$, and 3) is well approximated by

$$I_j \propto \frac{NP_j(e^{-(j-1)h\nu/k_B T} - e^{-jh\nu/k_B T})}{\sum_{i=1}^4 e^{-(i-1)h\nu/k_B T}}, \quad (2)$$

where N , k_B , h , ν , and P_j are the concentration of the paramagnetic center, Boltzmann's constant, Planck's constant, the microwave frequency employed, and the transition probability of the transition at B_j , respectively. For T_{V2a} and T_{V2b} , the temperature dependence of the sum of the intensities of the $|3/2, \pm 3/2\rangle \leftrightarrow |3/2, \pm 1/2\rangle$ transitions observed ($\mathbf{B}_0 \parallel [0001]$) was fitted to one calculated from Eq. (2) by least squares method with $\nu=9.438$ GHz used in the experiment. A good fitting shown in Fig. 5 suggests that the T_{V2a} and T_{V2b} spectra arise from the electronic ground state. It is established that the V_{Si}^- spectrum arises from the electronic ground state.⁷ In V_{Si}^- , the four M_S levels are equally spaced since the three $\Delta M_S = \pm 1$ transitions are superimposed. The temperature dependence of the signal intensity of V_{Si}^- was

well fitted to one calculated as the sum of the three $\Delta M_S = \pm 1$ transitions by using Eq. (2). In the temperature range studied ($125 \text{ K} \leq T$), Eq. (2) is further simplified to

$$I_j \propto \frac{NP_j h \nu}{k_B T} \frac{1}{\{4 - (6h\nu/k_B T)\}} \quad (3)$$

As shown in Fig. 5, the signal intensity varies linearly with $1/T$ in the temperature studied ($125 \text{ K} \leq T$). The difference of the gradient among the centers arises from the difference in the spin concentration and from the difference in the number of transitions summed to estimate the intensity. In V_{Si}^- , the signals of the $|3/2, \pm 3/2\rangle \leftrightarrow |3/2, \pm 1/2\rangle$ transitions of V_{Si}^- , which are too broadened to be observed as separate signals and constitute a part of the foot of the V_{Si}^- signal, were likely to be included in the estimation of the intensity obtained by double integration.

We fitted the temperature dependence of the signal intensity in the limited temperature range of $125 \text{ K} \leq T \leq 300 \text{ K}$, since it was difficult to measure quantitatively the signal intensity in low temperatures due to the saturation effect and the passage effect. The increase of the signal intensity with the decrease of the temperature in the range of $125 \text{ K} \leq T \leq 300 \text{ K}$ alone cannot exclude a possibility that T_{V2a} might arise from a low-lying electronic excited state. By using the equation for the temperature dependence of the signal intensity of a thermally accessible electronic excited state,²⁷ we note that the linear increase of the signal intensity with $1/T$ in this limited temperature range is applicable not only for an EPR signal from an electronic ground state but also for that from a low-lying electronic excited state with an energy higher than the electronic ground state by $\Delta E \leq \sim 0.005$ eV, where ΔE is the energy separation from the electronic ground state. Since the T_{V2a} signal was observed at 10 K, it is determined that the T_{V2a} signal arises from an electronic ground state.

The concentration of a defect at the particular charge state might depend on the temperature dependence of the position of the Fermi level. In our sample, the concentration of V_{Si}^- , which is the dominant defect created by the electron irradiation, was estimated to be similar to the carrier concentration at room temperature before the electron irradiation. The EPR signal of the nitrogen donor, which had been the dominant EPR signal before the electron irradiation, could not be observed after the electron irradiation. It is likely that an electron is transferred from nitrogen to V_{Si}^- . This indicates that the Fermi level lies around the center of the band gap after the electron irradiation. In this situation, it is likely that the Fermi level position does not depend on the temperature. We note that the signal intensity ratios T_{V2a}/V_{Si}^- and T_{V2b}/V_{Si}^- are constant above 170 K ($1/T = 5.88 \times 10^{-3} \text{ K}^{-1}$). The spin concentrations of V_{Si}^- , T_{V2a} , and T_{V2b} with the assignment of $S=3/2$, were estimated to be $5 \times 10^{17}/\text{cm}^3$, $5 \times 10^{16}/\text{cm}^3$, and $2 \times 10^{16}/\text{cm}^3$, respectively.

C. EPR parameters

1. Spin polarization

The C_{3v} symmetry and the EPR parameters \mathbf{g} and \mathbf{D} (with the assignment of $S=1$), and the ^{29}Si hyperfine coupling

constant of 12 NNN atoms of T_{V2a} were reported by the ODMR.¹⁶ However, the ^{13}C hyperfine splittings of NN atoms, which are crucial in identifying silicon vacancy, were not observed.^{28,29} In our electron-irradiated sample, the height of the signal intensity of T_{V2a} is 43 times smaller than that of V_{Si}^- . As seen from the spectrum in Fig. 1(a), many weak unidentified signals were observed besides the signals of V_{Si}^- , T_{V2a} , and T_{V2b} . The signal intensities of these weak signals correspond to several percentages of that of the primary lines of T_{V2a} and interfere with measuring the angular dependencies of the hyperfine lines of NN atoms. The selective enhancement of the EPR signal of T_{V2a} enabled us to measure the ^{13}C hyperfine splittings. In Figs. 1(b) and 1(c), the EPR spectra $\mathbf{B}_0 \parallel [0001]$ taken under the laser illumination (808 nm, 1.53 eV) are shown. The EPR signal of T_{V2a} was selectively enhanced through the spin polarization of the multiplet sublevels. In Fig. 1(b), the strong signal in the central part is considered to be arising mostly from that of V_{Si}^- because the intensity is similar to that in the dark. We note that the lineshape of the EPR spectrum of T_{V2a} under laser illumination exhibits mixed phase, absorptive in the low field line and emissive in the high field line and that the signal height of the $|3/2, \pm 3/2\rangle \leftrightarrow |3/2, \pm 1/2\rangle$ transitions of T_{V2a} matches that of V_{Si}^- . When the power of the laser light was decreased, the peak height of the $|3/2, \pm 3/2\rangle \leftrightarrow |3/2, \pm 1/2\rangle$ transitions of T_{V2a} decreased, while that of V_{Si}^- was similar to that in the dark, as shown in Fig. 1(c). In the spectrum under illumination, the central line (the $|3/2, 1/2\rangle \leftrightarrow |3/2, -1/2\rangle$ transition), which is as weak as that in the dark is hidden underneath the V_{Si}^- signal.

The pattern of the polarized spectrum ($\mathbf{B}_0 \parallel [0001]$) of T_{V2a} indicates that either the $M_S = \pm 1/2$ levels or the $M_S = \pm 3/2$ levels should be preferentially populated, with little population difference both between the $M_S = \pm 1/2$ levels and between the $M_S = \pm 3/2$ levels, but with a large population difference between the $M_S = \pm 1/2$ levels and the $M_S = \pm 3/2$ levels. In three unpaired electron system, the effective spin of electronic excited states is either $S = 1/2$ or $3/2$. Since a low-field line of absorption form and a high-field line of emission form are nearly the same peak height, and since the $|3/2, 1/2\rangle \leftrightarrow |3/2, -1/2\rangle$ transition is only slightly polarized, we assume that spin polarization should occur through an intersystem crossing from the excited doublet state to the Zeeman sublevels of the ground quartet state due to the spin-orbit mechanism. It is likely that the ground quartet state Q_0 is excited to an excited quartet state Q_1 by the laser light, and then transfers to an excited doublet state D , as shown in Fig. 6.

Upon the rotation with $\mathbf{B}_0 \perp [11\bar{2}0]$, the peak height of the polarized signals varies with the variation of the splitting between the $|3/2, \pm 3/2\rangle \leftrightarrow |3/2, \pm 1/2\rangle$ transitions, with the maximum at $\mathbf{B}_0 \parallel [0001]$ ($\theta' = 0$) and with the minimum (little polarization) at $\theta' \sim 55^\circ$. The pattern of the polarized spectrum in which the low-field line of the absorptive line shape and the high-field line of the emissive line shape had nearly the same peak height did not vary upon the rotation from $\mathbf{B}_0 \parallel [0001]$ to $\mathbf{B}_0 \parallel [1\bar{1}00]$. The central line of the $|3/2, 1/2\rangle \leftrightarrow |3/2, -1/2\rangle$ transition remained slightly polarized upon

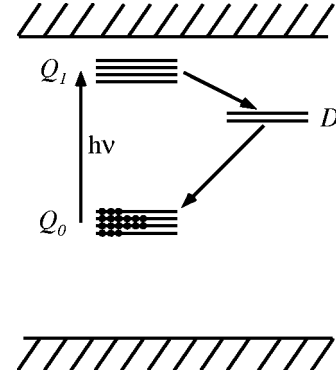


FIG. 6. Schematic illustration of the suggested model of the polarization mechanism. Q_0 , Q_1 , and D represent the ground quartet state, the excited quartet state, and the excited doublet state, respectively. The arrows indicate the suggested path which causes the polarization. The filled circles are the schematic representation of the populations of the ground state sublevels of a stationary state under illumination. Here, an example of the case that the $M_S = \pm 1/2$ levels are preferentially populated is illustrated. It should be noted that the $|3/2, \pm 3/2\rangle \leftrightarrow |3/2, \pm 1/2\rangle$ transitions are polarized strongly while the $|3/2, +1/2\rangle \leftrightarrow |3/2, -1/2\rangle$ transition is not polarized.

the rotation from $\mathbf{B}_0 \parallel [0001]$ to $\mathbf{B}_0 \parallel [1\bar{1}00]$. Since the T_{V2a} center has an isotropic g and a zero-field splitting which is smaller by two orders of magnitude than the Zeeman interaction $g\beta_e B$ at the microwave frequency of the X band, the mixing of different M_S states in the spin eigenfunctions of the ground quartet state is small in any direction of the external magnetic field. It is likely that this specific feature of the T_{V2a} center might cause the $|3/2, 1/2\rangle \leftrightarrow |3/2, -1/2\rangle$ transition to be little enhanced in any direction of the external magnetic field.

In the case of a polarization of the triplet ($S = 1$) through the intersystem crossing due to the spin-orbit mechanism, either the $M_S = \pm 1$ levels or the $M_S = 0$ level are preferentially populated with no population difference between the $M_S = \pm 1$ levels when the external magnetic field (\mathbf{B}_0) is along the principal axis Z of the zero-field splitting \mathbf{D} , when \mathbf{D} is axially symmetric. In this case, the two $M_S = \pm 1$ transitions have the same peak height and one exhibits an absorptive line shape and the other an emissive line shape. Both pattern of the polarized spectrum and the strength of the polarization depend on the angle between \mathbf{B}_0 and Z , since the M_S states are mixed in the eigenfunctions of the spin Hamiltonian at an arbitrary direction of the magnetic field. The degree of the mixing depends on the relative amplitude between the zero-field splitting and the Zeeman interaction. It has been shown that the two $M_S = \pm 1$ transitions have the same peak height, and one exhibits an absorptive line shape and the other an emissive line shape in any direction of the magnetic field when the zero-field splitting $|D|$ is very small compared to the Zeeman interaction.³⁰ In the case of a quartet arising from a doublet-triplet pair with a relatively small zero-field splitting ($|D| = 87$ MHz, $|E| = 0$), it was confirmed by the simulation of the polarization calculated by using the first-order perturbation approximation that the $|3/2, 1/2\rangle$

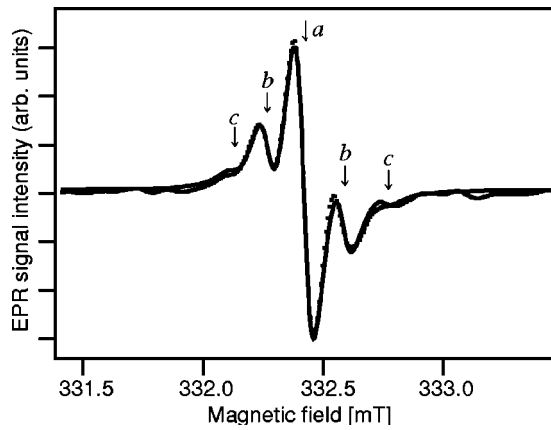


FIG. 7. The ^{29}Si hyperfine coupled signals of T_{V2a} in n -type $4H$ -SiC. The lowest field primary line with the magnetic field along the $[0001]$ axis is shown. The observed spectrum is indicated by the dotted line. The assignments of the hyperfine lines b and c are described in the text. The solid line indicates the simulated spectrum that is derived from the occupation of ^{29}Si ($I=1/2$, natural abundance 4.7%) at the 12 NNN silicon sites.

$\rangle \Leftrightarrow |3/2, -1/2\rangle$ transition is only slightly enhanced in any direction of the magnetic field.¹⁹

In the theoretical studies, the intravacancy transition energy of V_{Si}^- is calculated to be 1.57 and 1.40 eV at cubic and hexagonal sites, respectively.³¹ Furthermore, the energy level position of V_{Si}^- is calculated to be 1.19 and 1.28 eV above the valence band at cubic and hexagonal sites, respectively.¹¹ If we assume that the energy level position of T_{V2a} is similar to that of V_{Si}^- , the energy of our laser illumination (808 nm, 1.53 eV) is not large enough to bring up to the conduction band, but is sufficient to excite the intravacancy transition of T_{V2a} because the band gap in $4H$ -SiC is estimated to be 3.26 eV.⁵

2. ^{29}Si hyperfine interaction of next-nearest-neighbor (NNN) atoms

First we have confirmed the ^{29}Si hyperfine interactions arising from 12 NNN atoms which were reported in an ODMR study.¹⁶ The ^{29}Si hyperfine lines which appear as shoulders of the primary line of the spectrum taken with $\mathbf{B}_0 \parallel [0001]$ are labeled b and c (Fig. 7). Using the natural abundance of ^{29}Si (4.6832%),³² it is calculated that the probability for one ^{29}Si atom among the 12 NNN atoms it is 0.3316, for two ^{29}Si atoms it is 0.0896, for three ^{29}Si atoms 0.01469, and for four ^{29}Si atoms 0.0016. Thus the intensity ratio of the ^{29}Si NNN hyperfine lines with respect to the central line labeled a is calculated to be 0.273 (b/a) and 0.037 (c/a), respectively. As shown in Fig. 7, the observed spectrum is simulated using the calculated intensity ratio and Lorentzian line shape, with a ^{29}Si hyperfine coupling constant of 8.7 MHz. From the angular dependence of the line positions of b and c , the ^{29}Si hyperfine interaction of the NNN Si atoms was estimated to be isotropic within the resolution of the EPR measurements.

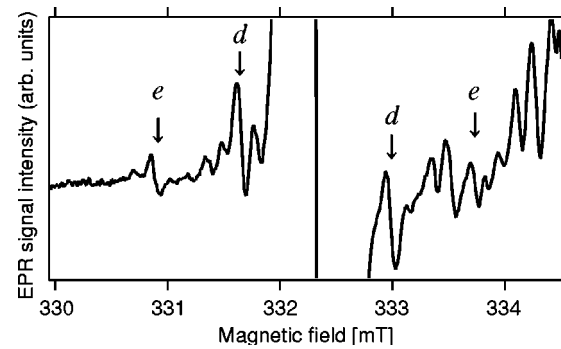


FIG. 8. The ^{13}C hyperfine satellites of T_{V2a} in n -type $4H$ -SiC with the magnetic field along the $[0001]$ axis. The lowest field primary line is shown. The labels d and e , for the assignment of the NN carbon sites, are described in the text.

3. ^{13}C hyperfine interaction of nearest-neighbor (NN) atoms

Now we report the observation of the ^{13}C hyperfine lines (Fig. 8 and 9). Weak satellite lines in the spectrum taken with $\mathbf{B}_0 \parallel [0001]$ are labeled d and e , as shown in Fig. 8. The intensity ratios of d and e with respect to the central line were 0.005 (d/a) and 0.016 (e/a), respectively. The signal inten-

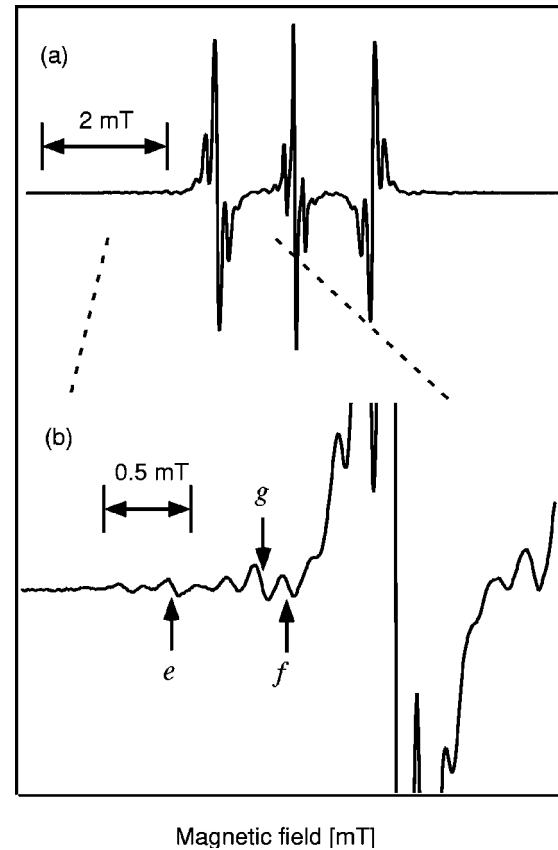


FIG. 9. The EPR spectrum of the electron-irradiated n -type $4H$ -SiC with the magnetic field parallel to the $[1\bar{1}00]$ axis under illumination with a laser light (808 nm) at 160 K (microwave power $0.2 \mu\text{W}$, amplitude of 100 kHz field modulation 0.03 mT, $\nu = 9.4203 \text{ GHz}$). (a) The whole spectrum. (b) The ^{13}C hyperfine components of the lowest field primary line.

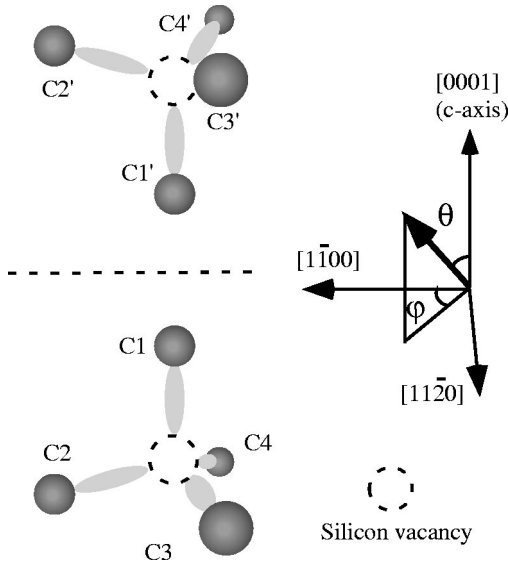


FIG. 10. The orientations of tetrahedra consisting of the NN carbon atoms. Since there are two magnetically distinguishable orientations, the two orientations illustrated here represent altogether four orientations in the lattice. The coordinate system used for the principal directions of the spin-Hamiltonian parameters is included. θ is the angle from the [0001] axis (c axis). φ is the angle from the [1100] axis in the (0001) plane.

sity ratio d/e is close to 3. The ratio $2(d+e)/a$ of 0.043 corresponds to the probability (0.0417) that one among the four carbons is occupied by ^{13}C , which has a natural abundance of 1.078%.³² With the C_{3v} symmetry, there is only one magnetically distinguishable site for the line positions of the primary lines which are determined by \mathbf{g} and \mathbf{D} . In a tetrahedron consisting of four carbon atoms around the silicon vacancy, the carbon atom (to be denoted axial carbon) which is located along [0001] and the three carbon atoms (to be denoted basal carbon atoms) in the basal plane are not symmetry related under the C_{3v} symmetry. Moreover, by utilizing the ^{13}C hyperfine lines which allows us to distinguish vacancy-carbon directions, two orientations of the tetrahedron are magnetically distinguishable. For the two orientations of the tetrahedron, there are altogether two axial carbon atoms labeled C1 and C1' in which the vacancy-carbon direction is along [0001] and six basal carbon atoms labeled C2–4 and C2'–4' (Fig. 10). Since the two axial atoms are not magnetically distinguishable, the hyperfine line e (Fig. 8 with $\mathbf{B}_0 \parallel [0001]$ and Fig. 9 with $\mathbf{B}_0 \parallel [1\bar{1}00]$) which arises from the two axial carbons does not split upon rotation. The six basal carbon atoms which are magnetically distinguishable are symmetry-related. The hyperfine line d (Fig. 8 with $\mathbf{B}_0 \parallel [0001]$) which is arises from the basal carbons splits into four lines with the intensity ratio 1:2:2:1 upon rotation with $\mathbf{B}_0 \perp [11\bar{2}0]$. With $\mathbf{B}_0 \parallel [1\bar{1}00]$, two sets of the basal carbons are magnetically distinguishable. In the spectrum with $\mathbf{B}_0 \parallel [1\bar{1}00]$ (Fig. 8), the hyperfine lines labeled f and g with the intensity ratio 2:4 are arising from the basal carbons.

The angular dependence of the line positions of ^{13}C hyperfine lines as well as that of the primary lines upon rotation

with $\mathbf{B}_0 \perp [11\bar{2}0]$ from $\mathbf{B}_0 \parallel [0001]$ to $\mathbf{B}_0 \parallel [1\bar{1}00]$ are shown in Fig. 11. Each point represents the line position observed. The angular dependence of the ^{13}C hyperfine splitting is shown in Fig. 12. The spin-Hamiltonian parameters were obtained by fitting observed field strengths and microwave frequencies to the spin Hamiltonian

$$\mathbf{H} = \beta_e \tilde{\mathbf{S}} \cdot \mathbf{g} \cdot \mathbf{B} + \tilde{\mathbf{S}} \cdot \mathbf{D} \cdot \mathbf{S} + \sum_i (\tilde{\mathbf{S}} \cdot \mathbf{A}_i \cdot \mathbf{I}_i - g_{ni} \beta_n \mathbf{I}_i \cdot \mathbf{B}), \quad (4)$$

where the electron spin $S=3/2$ and the nuclear spin $I=1/2$ for ^{13}C ($g_n=1.40483$)²⁷ and ^{29}Si ($g_n=-1.1106$).²⁷ \mathbf{g} , \mathbf{D} , and \mathbf{A} denote the g matrix, the ZFS tensor, and the hyperfine matrix, respectively. The subscripts i denote any of these nuclei. The least squares fitting was carried out by using computer program EPR.FOR in which the resonant magnetic fields are calculated by exact diagonalization of the spin Hamiltonian matrix. The spin Hamiltonian parameters were obtained by using a crystal coordinate system in which the z axis is [0001] and the x axis is [1 $\bar{1}$ 00]. One rotation with \mathbf{B}_0 in the (11 $\bar{2}$ 0) plane is sufficient to determine \mathbf{g} , \mathbf{D} , and \mathbf{A} of the axial carbon A^{13}C (C1), which have a C_{3v} symmetry. In the case of the basal carbons, \mathbf{A} of the C2 site A^{13}C (C2) was determined by applying the appropriate symmetry transformations to utilize the line positions of other sites as the line positions that should be obtained for the C2 site by the rotation in different planes. The results are summarized in Table II. For the basal carbons, the parameters of one particular site, C2 which is located on (11 $\bar{2}$ 0), are given. By applying the appropriate symmetry transformations, the parameters belonging to other basal carbon sites can be obtained. For the least-squares fitting, the line positions read from the spectra taken at every 2.5° were used. The parameters \mathbf{g} and \mathbf{D} were obtained from the primary lines. The number of measured line positions used for fitting and the root-mean-square deviations achieved are included in Table II. The solid curves in Figs. 11 and 12 are calculated by using the parameters obtained. As shown in Table II, the EPR parameters \mathbf{g} and \mathbf{D} and the ^{29}Si hyperfine coupling constant of the NNN atoms ($A_{iso}\text{Si}_{\text{NNN}}$) agree with those reported in the literature,¹⁶ except that \mathbf{D} in the latter was obtained with the assignment of $S=1$. The EPR parameters \mathbf{g} and \mathbf{D} of T_{V2b} obtained are listed in Table II.

D. Model of the T_{V2a} center

The wave function of the unpaired electron is described by a linear combination of atomic orbitals approximation

$$\Psi = \sum_i \eta_i (\alpha_i \varphi_{nsi} + \beta_i \varphi_{npi}), \quad (5)$$

where the summation is over the surrounding carbon (ns , np : $2s$, $2p$) and silicon (ns , np : $3s$, $3p$) atoms on which the unpaired electrons are delocalized. The fractional unpaired electron population (η_i^2) on the atom concerned and the hybrid ratio (β_i^2/α_i^2 , where $\alpha_i^2 + \beta_i^2 = 1$) are estimated from the hyperfine parameters. The results are listed in Table III. In the wave function of the unpaired electron, 62.3% of

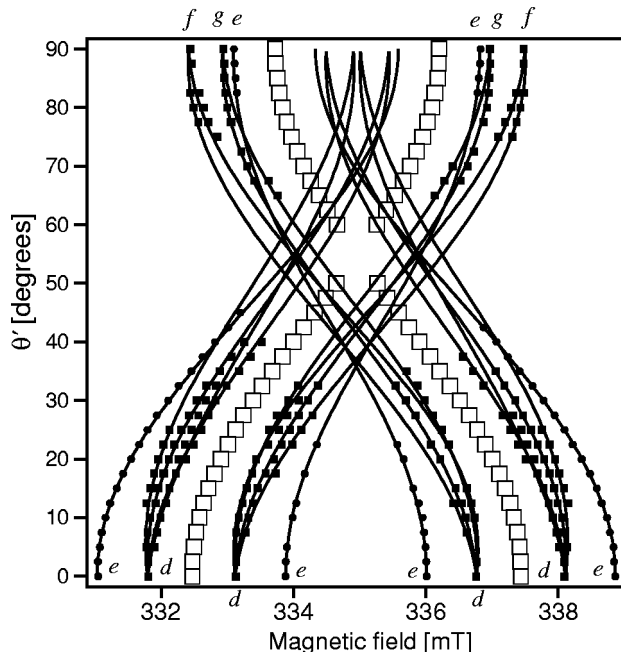


FIG. 11. Angular dependence of the line positions of T_{V2a} . The crystal was rotated with the magnetic field in the $(11\bar{2}0)$ plane (from $\theta' = 0^\circ$ for $\mathbf{B}_0 \parallel [0001]$ to $\theta' = 90^\circ$ for $\mathbf{B}_0 \parallel [1\bar{1}00]$). The open squares, the filled circles, and the filled squares represent the primary lines, the ^{13}C hyperfine lines of the axial carbon sites, and the ^{13}C hyperfine lines of the basal carbon site, respectively. The solid curves are calculated from the spin Hamiltonian parameters obtained.

the unpaired electron localizes on the four NN carbon atoms and 2.3% on the 12 NNN silicon atoms. The rest are likely to be on the surrounding carbon and silicon atoms. In the estimation ($\eta_i^2 \alpha_i^2 a_0 = A_{iso}$, $\eta_i^2 \beta_i^2 b_0 = A_{aniso}$), we used $a_0 = 3776.92$ MHz and $b_0 = 107.39$ MHz for ^{13}C , and $a_0 = -4594.12$ MHz for ^{29}Si .^{27,33} We note that the contribution to the wave function of the unpaired electron from the atomic orbital of carbon is almost purely p like (Table III). The dominant structure relaxation in T_{V2a} is likely to be outward displacements of the NN atoms.

The T_{V2a} center has a C_{3v} symmetry. From the small ZFS, the degree of distortion from T_d is considered to be very small. In $\mathbf{A}^{13}\text{C}$ of the basal carbon, the principal axis associated with the largest absolute principal value is denoted herein as the unique axis. In the basal carbon, the angle ($107.5^\circ \pm 0.3^\circ$) between $[0001]$ and the unique axis of $\mathbf{A}^{13}\text{C}$, which indicates the direction of the $2p$ orbital, is close to the tetrahedral angle (109.5°). Since the orbital parameters η^2 and β^2/α^2 of the axial carbon is similar to those of the basal carbon, the degree of the inequivalence between the axial and the basal carbon is very small. Since the NN atoms are four carbon atoms arranged in a configuration close to regular tetrahedron, since these carbons have a relatively large spin density, since the NNN atoms are 12 silicon atoms, and since the effective spin of T_{V2a} is $S = 3/2$, it is unambiguously identified that the T_{V2a} center belongs to a family of the negatively charged silicon vacancy. The g value, the ^{13}C

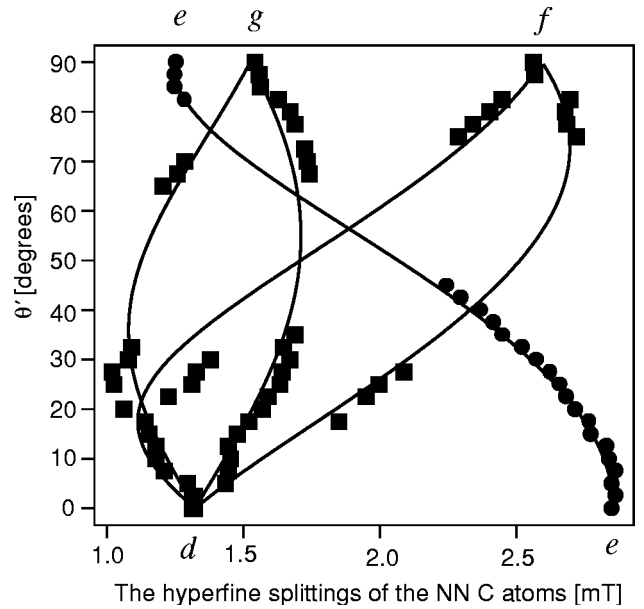


FIG. 12. Angular dependence of the ^{13}C hyperfine splittings of the NN carbon sites. The crystal was rotated with the magnetic field in the $(11\bar{2}0)$ plane (from $\theta' = 0^\circ$ for $\mathbf{B}_0 \parallel [0001]$ to $\theta' = 90^\circ$ for $\mathbf{B}_0 \parallel [1\bar{1}00]$). The filled circles and the filled squares represent the axial carbon sites and the basal carbon sites, respectively. The solid curves are calculated from the spin Hamiltonian parameters obtained.

hyperfine splittings of four NN carbons, and the ^{29}Si hyperfine splitting of the NNN atoms of T_{V2a} are similar to those of V_{Si}^- (Tables II and III).

It has been considered that not only the V_{Si}^- center in 3C-SiC but also those in 4H-SiC and in 6H-SiC have a T_d symmetry which makes the ZFS vanish.^{7,8} The criterion between nondistorted (V_{Si}^-) and distorted (V_{Si}^-) forms in the nutation experiments lies on the relative magnitude between $|D|$ and B_1 . For V_{Si}^- in 4H-SiC, in addition to nondistorted form in which all three $\Delta M_S = \pm 1$ transitions are simultaneously excited by the microwave pulse, the presence of a distorted configuration in which the ZFS exceeds the excitation band width ($B_1 \sim 0.3$ mT) of the microwave pulse employed was revealed. Since the outer two lines $|3/2, \pm 3/2\rangle \leftrightarrow |3/2, \pm 1/2\rangle$ of the distorted configuration could not be observed in both cw and pulsed experiments, these lines are likely to be broadened by a distribution of the ZFS. The distortion of the random character is likely to originate from lattice strains and/or site-to-site variation of the locations of nearby impurities and defects. The similar behavior in the nutation experiments was observed in the substitutional Ni^- center ($S = 3/2$) in diamond.²⁰

The T_{V2a} center which is also a negatively charged silicon vacancy is an analogue of V_{Si}^- . In the cases of T_{V2a} , the magnitude of the ZFS can be defined with a relatively narrow distribution (the linewidth ΔB_{pp} of 0.08 mT at 160 K). In our experiments, the origin of the distortion of the crystal field of T_{V2a} was not determined. Probably, the distortion might be caused by presence of some nonparamagnetic point defect such as a positively charged nitrogen, an interstitial

TABLE II. EPR parameters of T_{V2a} and T_{V2b} .

Defect	Principal values	Principal directions	T/K	comments
T_{V2a}				
\mathbf{g}^a	$g_{iso} = 2.0029 \pm 0.0001$		160	This work
\mathbf{g}	$g_{iso} = 2.004 \pm 0.002$		2	Ref. 16
\mathbf{g}	$g_{iso} = 2.0032$		300	Ref. 15
\mathbf{D}^a (MHz)	$ D = 35.1 \pm 0.1, E = 0^b$ ($ D = 70.1$ when $S = 1$)	$[0001]$ ($\theta = 0^\circ$) ^c	160	This work
\mathbf{D} (MHz)	$ D = 70 \pm 0.5$ ($S = 1$)	$[0001]$ ($\theta = 0^\circ$) ^c	2	Ref. 16
\mathbf{D} (MHz)	$ D = 66$ ($S = 1$)	$[0001]$ ($\theta = 0^\circ$) ^c	300	Ref. 15
$\mathbf{A}^{13}\text{C}(\text{C1})^a$ (MHz)	$A_{\parallel}\text{C}(\text{C1}) = 80.3 \pm 0.1$ $A_{\perp}\text{C}(\text{C1}) = 34.8 \pm 0.2$	$[0001]$ ($\theta = 0^\circ$) ^c $\theta = 90^\circ$	160 160	This work This work
$\mathbf{A}^{13}\text{C}(\text{C2})^a$ (MHz)	$A_x\text{C}(\text{C2}) = 75.8 \pm 0.4$ $A_y\text{C}(\text{C2}) = 31.3 \pm 0.2$ $A_z\text{C}(\text{C2}) = 27.2 \pm 0.6$	$\theta = 107.5^\circ \pm 0.3^\circ, \phi = 0^\circ \pm 0.3^\circ$ $\theta = 17.5^\circ \pm 0.3^\circ, \phi = 0^\circ \pm 1.3^\circ$ $\theta = 90^\circ \pm 3.8^\circ, \phi = 90^\circ \pm 1.2^\circ$	160 160 160	This work This work This work
$\mathbf{A}^{29}\text{Si}_{\text{NNN}}$ (MHz)	$A_{iso}\text{Si}_{\text{NNN}} = 8.7 \pm 0.1$		160	This work
T_{V2b}				
\mathbf{g}	$g_{iso} = 2.0029 \pm 0.0001$		160	This work
\mathbf{g}	$g_{iso} = 2.004 \pm 0.002$		2	Ref. 16
\mathbf{g}	$g_{iso} = 2.0032$		300	Ref. 15
\mathbf{D} (MHz)	$ D = 20.0 \pm 0.5, E = 0$ ($ D = 40.0$ when $S = 1$)	$[0001]$ ($\theta = 0^\circ$) ^c	160	This work
\mathbf{D} (MHz)	$ D = 36 \pm 0.5$ ($S = 1$)	$[0001]$ ($\theta = 0^\circ$) ^c	2	Ref. 16
\mathbf{D} (MHz)	$ D = 39$ ($S = 1$)	$[0001]$ ($\theta = 0^\circ$) ^c	300	Ref. 15
[1.5mm] V_{Si}^-				
\mathbf{g}	$g_{iso} = 2.0028 \pm 0.0001$		160	This work (Ref. 25)

^aThe number of the measured line positions used are 68 from the primary lines, 61 from the ^{13}C hyperfine lines of the axial carbon site, and 175 from the ^{13}C hyperfine lines of the basal carbon sites for the fitting of (1) \mathbf{g} and \mathbf{D} , (2) $\mathbf{A}^{13}\text{C}(\text{C1})$, and (3) $\mathbf{A}^{13}\text{C}(\text{C2})$, respectively. The root-mean-square deviation (mT) achieved are 0.007, 0.01, and 0.03 for (1) the primary lines, (2) the ^{13}C hyperfine lines of the axial carbon site, and (3) the ^{13}C hyperfine lines of the basal carbon sites, respectively.

^bThe ZFS parameter D and E are obtained from the relationships, $D = -3/2D_{zz}$ and $E = 1/2(D_{xx} - D_{yy})$.

^cAxially symmetric about $[0001]$.

silicon atom, or a carbon vacancy located at a certain distance away from the vacancy along $[0001]$. Although the ^{13}C hyperfine interaction has not been measured, T_{V2b} is likely to be another analog of V_{Si}^- in which either the kind or the location of the accompanying defect is different from T_{V2a} . A silicon vacancy-related $S = 3/2$ defect having C_{3v} symme-

try with the ZFS $|D| = 68.7 \times 10^{-4} \text{ cm}^{-1}$ (206 MHz) was found in p -type $6H$ -SiC irradiated with low-energy electrons (300 keV).³⁴ In this case, three $\Delta M_S = \pm 1$ transitions were clearly observed without being interfered by any other dominant signals. A model of a Frenkel pair (a pair of silicon vacancy and an interstitial silicon atom) was suggested.

In $4H$ -SiC, it is expected that two types of silicon vacancies should be produced, each corresponds to each of two types of silicon sites, one with cubic character and the other with hexagonal character. For both the V_{Si}^- and T_{V2a} spectra, it has not been determined whether the silicon vacancy corresponds to one of the two types of silicon sites or the resolution of our EPR technique is not sufficient to resolve the two spectra, each arising from each of two kinds of silicon vacancies.

In V_{Si}^- which is a negatively charged silicon vacancy of the T_d symmetry, the high-spin state $S = 3/2$ is arising from three parallel spins in the threefold-degenerate t_2 orbitals. This configuration with the three electrons in three different orbitals minimizes the electron repulsion by allowing the electrons stay far apart. The conservation of the T_d symmetry is ascribed to the orbitally nondegenerate 4A_2 state ($a_1^2 t_2^3$)

TABLE III. Hyperfine and orbital parameters of T_{V2a} .

	A_{iso} (MHz)	A_{aniso} (MHz)	η^2	β^2/α^2
$\mathbf{A}^{13}\text{C}(\text{C1})$	50.0 ± 0.1	15.1 ± 0.1	0.154	10.7
$\mathbf{A}^{13}\text{C}(\text{C2-4})$	44.8 ± 0.5	15.5 ± 0.2	0.156	12.2
$\mathbf{A}^{13}\text{C}(V_{Si}^-)^a$	49.3	15.4	0.157	11.0
$\mathbf{A}^{29}\text{Si}_{\text{NNN}}$	8.7 ± 0.1	0 ± 0.1	0.0019	
$\mathbf{A}^{29}\text{Si}_{\text{NNN}}^b$	8.35	0	0.0018	
$\mathbf{A}^{29}\text{Si}_{\text{NNN}}^c$	8.5	0	0.0019	

^a $\mathbf{A}^{13}\text{C}(V_{Si}^-)$ indicates the ^{13}C hyperfine matrix of the NN atoms of the V_{Si}^- reported in Ref. 7.

^b $\mathbf{A}^{29}\text{Si}_{\text{NNN}}$ of V_{Si}^- reported in Ref. 7.

^c $\mathbf{A}^{29}\text{Si}_{\text{NNN}}$ of T_{V2a} reported in Ref. 16.

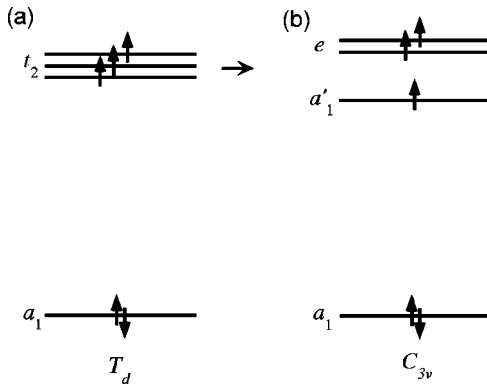


FIG. 13. Schematic energy levels of the negatively charged silicon vacancy in the one-electron molecular orbital approach for (a) T_d and (b) C_{3v} . It is assumed here that a'_1 is lower in energy than e .

which is not subject to a Jahn-Teller distortion. The T_{V2a} center is a negatively charged silicon vacancy of the C_{3v} symmetry. The distortion from a regular tetrahedron in T_{V2a} is evidenced by the ZFS, by the difference of the principal values of $\mathbf{A}^{13}\text{C}$ between the axial and the basal carbon sites, and by the principal directions of $\mathbf{A}^{13}\text{C}$ of the basal carbon. Under the C_{3v} symmetry, the t_2 triplet under the T_d symmetry splits into an a'_1 singlet and an e doublet as shown in Fig. 13. The spin quartet state ($S=3/2$) is not obtained from an electronic configuration either $a'_1{}^2e$ or e^3 . The configuration a'_1e^2 gives rise to the states 2A_1 , 4A_2 , and 2E , as inferred from the decomposition of the direct product of $A_1 \times E \times E$.³⁵ Thus the T_{V2a} spectrum arises from the ground state 4A_2 . We could not determine which of the orbitals, a'_1 or e , is lower in energy. Thus, the 4A_2 state might be either a'_1e^2 or $e^2a'_1$. Since 4A_2 is an orbitally nondegenerate state which is not subject to the Jahn-Teller effect, a further symmetry-lowering distortion from C_{3v} is not required. The high-spin configuration is attained since the reduction of the electronic repulsion by occupying three different orbitals is larger than the energy gain obtained from the crystal field splitting. We note that three parallel spins are occupied in three different orbitals among which a'_1 and two orbitals of the e doublet are different in energy. The strong localization of unpaired electrons on the NN atoms in both V_{Si}^- and T_{V2a} suggests that electron repulsion should be the predominant factor in determining the electronic structure of a silicon vacancy in SiC. It should be mentioned that the high-spin many-electron 4A_2 state is favorable not only due to the reduction of the electron repulsion but also due to the energy gain due to electron exchange. We think the role of many-

electron effect in determining the ground state configuration is demonstrated clearly in T_{V2a} which does have the crystal field splitting competing against the many-electron effect.

IV. SUMMARY

The T_{V2a} center in electron irradiated n -4H-SiC, for which a structural model was not established, has been studied by cw- and pulsed EPR. We have assigned our spectra to arise from the T_{V2a} center since the EPR parameters agree with those reported.^{15,16} From the temperature dependence of the EPR signal intensity at thermal equilibrium, it has been determined that both spectra T_{V2a} and T_{V2b} arise from the ground state. The spin multiplicity of T_{V2a} and T_{V2b} has been determined to be quartet ($S=3/2$) by the nutation method of pulsed EPR. By enhancing the EPR signals of T_{V2a} with illumination of the laser light (808 nm), $\mathbf{A}^{13}\text{C}$'s of the four NN carbon atoms of T_{V2a} have been determined. The EPR parameters \mathbf{g} , \mathbf{D} , and $A_{iso}\text{Si}_{NNN}$ obtained in the present work agree with those reported in the literature, except that \mathbf{D} was obtained with the assignment of $S=1$ in the latter. Since the NN atoms are four carbon atoms arranged in a configuration close to a regular tetrahedron, since these carbons have a relatively large spin density (62.3%), since the NNN atoms are 12 silicon atoms, and since the effective spin is $S=3/2$, the T_{V2a} center has been identified as an analog of a negatively charged silicon vacancy V_{Si}^- . Thus the T_{V2a} spectrum arises from the ground state 4A_2 of a negatively charged silicon vacancy with C_{3v} symmetry. The symmetry-lowering distortion from T_d to C_{3v} , which is inferred to be small from the small $|\mathbf{D}|$ and the similarity of the principal values of $\mathbf{A}^{13}\text{C}$ between axial and basal carbon, is likely to be caused by a perturbation of the crystal field, and possibly by the presence of an accompanying impurity or defect. The vacancies reported to have a high-spin 4A_2 ground state in which the many-electron effect dominates over the energy gain attained by a Jahn-Teller distortion are limited to those having T_d symmetry.^{2,6,36,37} It should be noted that T_{V2a} is the case in which three parallel spins are occupied in three orbitals, among which a'_1 and two orbitals of the e doublet are split by the crystal field of the C_{3v} symmetry.

ACKNOWLEDGMENTS

This work was performed under the management of FED as a part of the METI Project (R&D of Ultra-Low-Loss Power Device Technologies) supported by NEDO. This work was partly supported by grants from the University of Library and Information Science Research Projects.

*Present address: Institute of Library and Information Science, University of Tsukuba, 1-2 Kasuga, Tsukuba-City, Ibaraki, 305-8550, Japan.

†Present address: Research Center for Knowledge Communities, University of Tsukuba, 1-2 Kasuga, Tsukuba-City, Ibaraki, 305-8550, Japan.

¹C. A. Coulson and M. J. Kearsley, Proc. R. Soc. London, Ser. A

241, 433 (1957).

²J. Isoya, H. Kanda, Y. Uchida, S. C. Lawson, S. Yamasaki, H. Itoh, and Y. Morita, Phys. Rev. B **45**, 1436 (1992).

³G. D. Watkins, in *Radiation Damage in Semiconductors*, edited by P. Baruch (Dunod, Paris, 1965), pp. 97–113.

⁴E. G. Sieverts, M. Sprenger, and C. A. J. Ammerlaan, Phys. Rev. B **41**, 8630 (1990).

- ⁵W. J. Choyke, D. R. Hamilton, and L. Patrick, *Phys. Rev.* **133**, A1163 (1964).
- ⁶H. Itoh, M. Yoshikawa, I. Nashiyama, S. Misawa, H. Okumura, and S. Yoshida, *IEEE Trans. Nucl. Sci.* **37**, 1732 (1990); H. Itoh, A. Kawasuso, T. Ohshima, M. Yoshikawa, I. Nashiyama, S. Tanigawa, S. Misawa, H. Okumura, and S. Yoshida, *Phys. Status Solidi A* **162**, 173 (1997).
- ⁷T. Wimbauer, B. K. Meyer, A. Hofstaetter, A. Scharmann, and H. Overhof, *Phys. Rev. B* **56**, 7384 (1997).
- ⁸J. Schneider and K. Maier, *Physica B* **185**, 199 (1993).
- ⁹H. Itoh, N. Hayakawa, I. Nashiyama, and E. Sakuma, *J. Appl. Phys.* **66**, 4529 (1989).
- ¹⁰L. Torpo, R. M. Nieminen, K. E. Laasonen, and S. Pöykkö, *Appl. Phys. Lett.* **74**, 221 (1999).
- ¹¹A. Zywiets, J. Furthmüller, and F. Bechstedt, *Phys. Rev. B* **59**, 15 166 (1999).
- ¹²A. Zywiets, J. Furthmüller, and F. Bechstedt, *Phys. Rev. B* **62**, 6854 (2000).
- ¹³V. S. Vainer, V. I. Veigner, V. A. Il'n, and V. F. Tsvetkov, *Fiz. Tverd. Tela (Leningrad)* **22**, 3436 (1980) [*Sov. Phys. Solid State* **22**, 2011 (1980)].
- ¹⁴V. S. Vainer and V. A. Il'n, *Fiz. Tverd. Tela (Leningrad)* **23**, 3659 (1981) [*Sov. Phys. Solid State* **23**, 2126 (1981)].
- ¹⁵H. J. von Bardeleben, J. L. Cantin, I. Vickridge, and G. Battistig, *Phys. Rev. B* **62**, 10 126 (2000).
- ¹⁶E. Sörman, N. T. Son, W. M. Chen, O. Kordina, C. Hallin, and E. Janzén, *Phys. Rev. B* **61**, 2613 (2000).
- ¹⁷N. Mizuochi, J. Isoya, S. Yamasaki, H. Takizawa, N. Morishita, T. Ohshima, and H. Itoh, *Mater. Sci. Forum* **389-393**, 497 (2002).
- ¹⁸K. Ishii, J. Fujisawa, A. Adachi, S. Yamauchi, and N. Kobayashi, *J. Am. Chem. Soc.* **120**, 3152 (1998).
- ¹⁹N. Mizuochi, Y. Ohba, and S. Yamauchi, *J. Chem. Phys.* **22**, 3479 (1999).
- ²⁰J. Isoya, H. Kanda, J. R. Norris, J. Tang, and M. K. Bowman, *Phys. Rev. B* **41**, 3905 (1990).
- ²¹A. V. Astashkin and A. Schweiger, *Chem. Phys. Lett.* **174**, 595 (1990).
- ²²B. G. Segal, M. Kaplan, and G. K. Fraenkel, *J. Chem. Phys.* **43**, 4191 (1965).
- ²³R. D. Allendoerfer, *J. Chem. Phys.* **55**, 3615 (1971).
- ²⁴T. Chang, D. Foster, and A. H. Kahn, *J. Res. Natl. Bur. Stand.* **83**, 133 (1978).
- ²⁵T. Wimbauer *et al.* estimated the g value of the negative silicon vacancy to be 2.0034 ± 0.0001 by calibrating the magnetic field with a proton resonance probe. (Ref. 7) In our measurement, the isotropic g value of the negatively charged vacancy at room temperature is determined to be 2.0028 ± 0.0001 by using perylene cation reference in conc. H_2SO_4 as described in the experiment section.
- ²⁶A. Abragam, in *The Principles of Nuclear Magnetism* (Clarendon Press, Oxford, 1961).
- ²⁷J. A. Weil, J. R. Bolton, and J. E. Wertz, in *Electron Paramagnetic Resonance* (Wiley, New York, 1994).
- ²⁸Preliminary results of the measurements of the ^{13}C hyperfine interactions of the NN atoms through the spin polarization by a laser light illumination by us (Ref. 17) and by using ODMR by Mt. Wagner *et al.* (Ref. 29) were reported.
- ²⁹Mt. Wagner, N. Q. Thinh, N. T. Son, P. G. Baranov, E. N. Mokhov, C. Hallin, W. M. Chen, and E. Janzén, *Mater. Sci. Forum* **389-393**, 501 (2002).
- ³⁰S. K. Wong, D. A. Hutchinson, and J. K. Wan, *J. Chem. Phys.* **58**, 985 (1973).
- ³¹A. Zywiets, J. Furthmüller, and F. Bechstedt, *Phys. Rev. B* **61**, 13 655 (2000).
- ³²G. Audi and A. H. Wapstra, *Nucl. Phys. A* **565**, 1 (1993).
- ³³J. R. Morton and K. F. Preston, *J. Magn. Reson.* **30**, 577 (1978).
- ³⁴H. J. von Bardeleben, J. L. Cantin, L. Henry, and M. F. Barthe, *Phys. Rev. B* **62**, 10 841 (2000).
- ³⁵F. A. Cotton, in *Chemical Applications of Group Theory*, 2nd ed. (Wiley, New York, 1971).
- ³⁶T. A. Kennedy and N. D. Wilsey *Phys. Rev. B* **23**, 6585 (1981); T. A. Kennedy, N. D. Wilsey, J. J. Krebs, and G. H. Stauss, *Phys. Rev. Lett.* **50**, 1281 (1983).
- ³⁷J. Hage, J. R. Niklas, and J.-M. Spaeth, *Mater. Sci. Forum* **10-12**, 259 (1986).